Available online at www.sciencedirect.com
SCIENCE DIRECT®
Journal of Power Sources 134 (2004) 1–6
JOURNAL OF POWER SOURCES
www.elsevier.com/locate/jpowsour

Synthesis and physical/electrochemical characterization of Pt/C nanocatalyst for polymer electrolyte fuel cells

J. Prabhuram, T.S. Zhao*, C.W. Wong, J.W. Guo

Department of Mechanical Engineering, Hong Kong University of Science and Technology, Clear Water Bay, Kowloon, Hong Kong

Received 29 January 2004; accepted 20 February 2004

Available online 25 May 2004

Abstract

In the present study, 20 wt.% Pt/C nanocatalyst has been synthesized by the simple formic acid reduction method (FARM) in the organic solvent tetrahyrofuran (THF). Transmission electron microscope (TEM) and X-ray diffraction (XRD) analyses indicate the formation of well-dispersed Pt nanoparticles having sizes of around 3–4 nm on the Vulcan XC-72 carbon support. A comparison between two different synthetic approaches by using the FARM shows that the formation and dispersion of the Pt nanoparticles can be facilitated by the THF solvent and high surface area Vulcan XC-72 carbon support. The surface characterization of the Pt/C by X-ray photoelectron spectroscopy (XPS) reveals that 60.3% of Pt is present in its metallic state. Furthermore, the electrochemical characterization by the cyclic voltammetry (CV) demonstrates that the electrochemical active surface (EAS) area and methanol oxidation reaction of the Pt/C is respectively almost similar and slightly higher than that of the 20 wt.% Pt/C E-TEK catalyst.

Keywords: Platinum nanocatalyst; Formic acid reduction method; Cyclic voltammetry; Electrochemical active surface area; Methanol oxidation

1. Introduction

The development of polymer electrolyte fuel cells (PEFCs) is mainly hampered by the factors such as sluggish electrochemical reaction on the catalytic surface and methanol crossover through the Nafion membranes in the case of usage of liquid methanol as a fuel [1,2]. The former problem is normally encountered due to the poor morphological structure of the catalyst layer, and this can be resolved by providing a high surface area of the Pt and its alloys on a carbon support. The high surface area of a Pt and its alloys can be rendered by using the nanocatalytic materials on a carbon support [3]. Hence, the synthetic aspects of nanoparticles of the Pt and its alloys on the carbon support have attracted much interest in view of their superior electro-catalytic activity for PEFC applications [4–8]. Recently, Zhou et al. [9] prepared uniform platinum nanoparticles with an average diameter of 2.9 nm on carbon by the polyol process and that exhibited a higher electro-catalytic activity for the oxygen reduction reaction. The nanoparticles of Pt/C, Pt–Ru/C and Pt–Ni/C alloys produced by microwave irradiation assisted by stabilizing agents showed higher electro-catalytic activity towards the methanol oxidation reaction [10–12]. Yang et al. [13] adopted the impregnation method to obtain 40 wt.% of Pt-RuO_xH_y/C nanocatalyst for the methanol oxidation reaction and suggested that the impregnation method imposes relatively lower surface oxidation states which is considered suitable for the methanol oxidation reaction. In the studies by Schmidt et al. [4] and Paulus et al. [5] well-dispersed Pt–Ru/C nanoparticles were synthesized by using the surfactants tetraalkylamonium bromide. Recently, we have been able to obtain well-dispersed Pt/C nanocatalyst (2–3 nm) that was stabilized by the surfactant, tetraoctylammonium bromide for PEFC applications [8]. From the above-mentioned investigations, it is understood that in most of the preparative methods, surfactants, polymers and ligands are involved in controlling the particle sizes, in addition to providing good dispersion on the supporting materials. Although the role of stabilizing agents in controlling the particles to a desired size is found to be crucial, their coverage over the surfaces of the catalytic particles hinders the chemisorption of reactants onto the catalytic particles, during electro-catalytic measurements. Hence, an additional treatment is required to get rid of these stabilizing molecules from surfaces, and this process is cumbersome in the preparation of the catalysts.

* Corresponding author. Tel.: +852-2358-8647; fax: +852-2358-1543.
E-mail address: metzhao@ust.hk (T.S. Zhao).

0378-7753/$ – see front matter © 2004 Elsevier B.V. All rights reserved.
doi:10.1016/j.jpowsour.2004.02.021

In this context, it is interesting to mention the study by Valbuena et al. [14], who followed the formic acid reduction method (FARM) in producing the Pt/C and Pt–Ru/C nanoparticles having sizes of around 5.5 nm without using any stabilizing agents in the aqueous media. It was suggested that the formic acid does not introduce any type of impurities to the catalysts, during the reduction process.

In the present study, we have adopted the FARM for the synthesis of 20 wt.% Pt/C nanocatalyst with the diameter of 3–4 nm in the organic solvent THF. The solvent THF has been chosen in this synthesis method because it has the tendency to stabilize the small metal particles, in addition to acting as a good dispersing media for the metal particles [15,16]. It has been shown that the electrochemical active surface (EAS) area of the in-house made 20 wt.% Pt/C is almost same to that of the 20 wt.% Pt/C E-TEK catalyst, while methanol oxidation current of the former is slightly higher than that of the latter.

2. Experimental

The 20 wt.% Pt/C nanocatalyst was synthesized by mixing appropriate amounts of precursor H_2PtCl_6 and Vulcan XC-72 carbon in the solvent THF and the mixture was ultrasonicated for 30 min. To this mixture, 40 ml of 98% of formic acid was added and refluxed at 90 °C for 6 h. After this process, the excess reducing agent and organic solvent present in the mixture were evaporated at 60 °C and dried in a vacuum oven overnight. Subsequently, the formed Pt/C catalyst was dispersed in an ethanol and water mixture and ultrasonicated for 30 min. Finally, it was filtered, washed with excess de-ionized water and dried in a vacuum oven at 70 °C for 2 h. Henceforth, this catalyst will be named as Pt/C-I.

For comparison, the 20 wt.% Pt/C catalyst was also synthesized by slightly modifying the above procedure, i.e., an appropriate amount of H_2PtCl_6 was taken in the solvent THF and 40 ml of 98% of formic acid was added and refluxed at 90 °C for 6 h. The excess reducing agent and organic solvent present in the mixture was evaporated at 60 °C and dried in a vacuum oven for overnight. The Pt colloids formed were dispersed in an ethanol and water mixture and then added to the Vulcan XC-72 carbon suspension with continuous stirring for 4 h. After that, it was filtered, washed with excess de-ionized water and dried in a vacuum oven at 70 °C for 2 h. Hereafter, this catalyst will be termed as Pt/C-II.

The physical characterization of the Pt/C nanocatalysts was carried out by high resolution TEM and XRD analyses. The TEM images were obtained by using high resolution JEOL 2010 TEM system operated with a LaB6 filament at 200 kV. The XRD patterns were obtained with Philips Powder Diffraction System (Model PW 1830) using and Cu Kα source operated at 40 keV a scan rate of $0.025^\circ\,s^{-1}$. The surface characterization was carried out by the XPS technique, which is equipped with a Physical Electronics PHI 5600 multi-technique system using Al monochromatic X-ray at a power of 350 W. The survey and regional spectra were obtained by passing energy of 187.85 and 23.5 eV, respectively.

The electrochemical characterization was carried out by the CV using a potentiostat (EG&G Princeton, Model 273 A) connected to a three electrode cell assembly with glassy carbon (GC) electrode as the working, Ag/AgCl as the reference and Pt wire as the counter electrodes, respectively. The GC electrode (4 mm diameter and 0.125 cm^2 area) was prepared by the procedure reported in our recent work [8]. Briefly, the GC electrode was polished to a mirror finish with 0.05 μm alumina suspension and served as an underlying substrate. The catalyst ink was prepared by ultrasonically dispersing 7.2 mg of 20 wt.% of Pt/C in 2.5 ml of ethanol, to which 0.5 ml of 0.1 wt.% of Nafion solution was added and the dispersion was then ultrasonicated for 30 min. A quantity of 10 μl catalyst ink was pipetted out and on the top of the GC substrate and over that 10 μl of 0.1 wt.% of Nafion was added. Then, the electrode was dried at 80 °C to yield a Pt loading of 48 $\mu g\,cm^{-2}$. The 0.1 M $HClO_4$ was used as an electrolyte and prepared by using ultrapure water (Millipore, 18 MΩ). N_2 gas was purged for nearly 30 min, before starting the experiment.

3. Results and discussion

3.1. Morphology of Pt/C nanocatalysts

Fig. 1 presents the high resolution TEM images of the 20 wt.% Pt/C nanocatalysts. The low magnification of the TEM image of the Pt/C-I catalyst shown in Fig. 1a indicates that the black color small Pt particles are well dispersed on the carbon support. And the highly magnified TEM image shown in Fig. 1b clearly displays the dispersed Pt fringes with mean diameters of 3–4 nm. On the other hand, in the Pt/C-II catalyst the small Pt particles undergo severe aggregations as shown in Fig. 1c. From the high magnification of the TEM image, as shown in Fig. 1d, one can see that how these small size Pt particles (ca. 4 nm) are aggregated on the one side of the carbon particle. The size of the Pt particles for the 20 wt.% Pt/C E-TEK catalyst is found to be around 2.6 nm from the TEM image (figure not shown).

In the Pt/C-I catalyst, the formation and good dispersion of the Pt nanoparticles can be explained by the phenomena that as soon as the Pt nucleuses are formed in the reduction process, they can be surrounded by the excess THF molecules, that can stabilize their growth and subsequently, adsorbed on the high external surface of the Vulcan XC-72 carbon (surface area is ca. 250 $m^2\,g^{-1}$) and in their macropores [17,18]. Earlier, Bonmann et al. [15] proved the stabilizing effect of the THF solvent on the Ti colloids, during their preparation of homogeneous Ti nanoparticles in excess of the THF solvent. From these results, it is deduced that the high surface area Vulcan XC-72 carbon can facilitate the

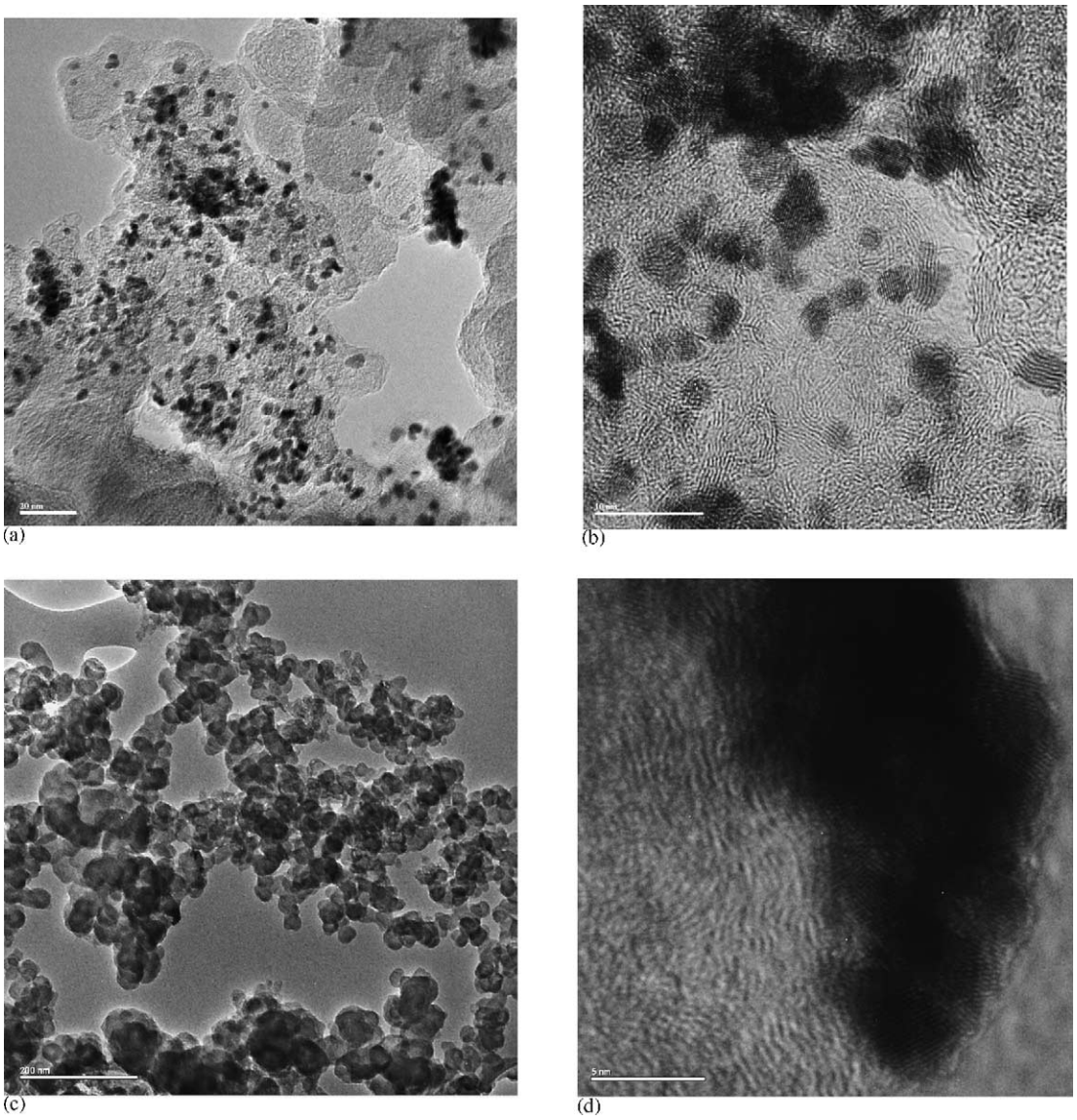

Fig. 1. TEM images of the 20 wt.% Pt/C nanocatalyst: (a) low-magnification TEM of Pt/C-I, (b) high-magnification TEM of Pt/C-I, (c) low-magnification TEM of Pt/C-II and (d) high-magnification TEM of Pt/C-II.

dispersion of small Pt particles over its surfaces. This view is consistent with the work by McBreen et al. [19] who reported that among the various types of carbons, the Vulcan XC-72 carbon yielded higher dispersion for the Pt particles on its surface.

In the case of Pt/C-II catalyst, an aggregation of the Pt particles on the carbon support might be possible because at one stage of the preparative process, the THF solvent is completely removed from the Pt colloidal solution before it is mixed with the Vulcan XC-72 carbon suspension. Consequently, the small bare (without the coverage of THF molecules) Pt particles can undergo a high degree of aggregation on the carbon support as displayed in the Fig. 1d.

The XRD patterns of the Pt/C-I, Pt/C-II and E-TEK catalysts are shown in Fig. 2. All the three catalysts exhibited characteristic diffraction peaks of Pt(1 1 1) at 2θ of 39.79°,

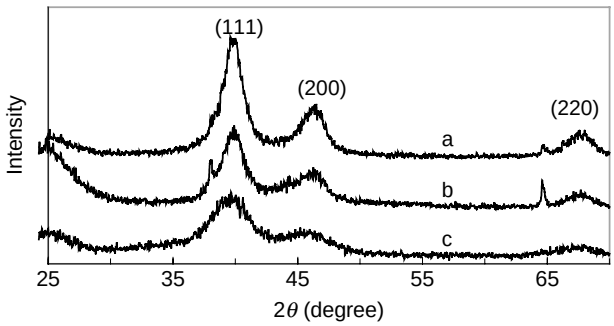

Fig. 2. XRD patterns of the 20 wt.% Pt/C: (a) Pt/C-I, (b) Pt/C-II and (c) E-TEK catalysts.

Table 1
Comparison of morphological data of the Pt/C-I, Pt/C-II and 20 wt.% Pt/C E-TEK catalysts

Catalysts	Particles size from TEM (nm)	Average particles size from XRD (nm)	Surface area ($m^2\ g^{-1}$)
Pt/C-I	3.5	4.10	81
Pt/C-II[a]	4.0	3.40	–
E-TEK	2.6	1.87	108

[a] Surface area not measured because of severe aggregation of the particles.

Pt(2 0 0) at 2θ of 46.3° and Pt(2 2 0) at 2θ of 67.45°, indicate that Pt is present in the face centered cubic (fcc) phase. The average sizes of the Pt particles are obtained by broadening the Pt(1 1 1) peak by using the Scherrer equation after background subtraction and the average particle sizes of the Pt/C-I, Pt/C-II and E-TEK catalysts are found to be 4.1, 3.4 and 1.87 nm, respectively. The average sizes of the particles of these catalysts are agreed well with the TEM results. The morphological data of the Pt/C-I, Pt/C-II and E-TEK catalysts are compared in Table 1. The surface areas of these catalysts are calculated from the mean diameter of the particles that are obtained from the TEM images by using the equation:

$$S = \frac{6000}{d\rho} \quad (1)$$

where S is the surface area ($m^2\ g^{-1}$), d the mean diameter of the particles (nm) and ρ is density of Pt (21.4 $g\ cm^{-3}$). The surface area of the Pt/C-I is slightly lower than the E-TEK catalyst due to its bigger particle diameter than that of the E-TEK. Though the size of the individual Pt particles can be obtained from the TEM image and XRD peak width for the Pt/C-II catalyst, an aggregated nature of the Pt particles does not allow measuring the surface area for this catalyst. Further discussions will be focused mainly on the well-dispersed Pt/C-I catalyst.

3.2. Surface characterization of Pt/C-I catalyst

The regional XPS of Pt(4f) core level of the Pt/C-I catalyst is shown in Fig. 3. The Pt(4f) region displays two doublets from the spin-orbital splitting of the $4f_{7/2}$ and $4f_{5/2}$ states. These doublets contain a low energy band centered at 70.9 eV and high energy band at 74.2 eV, indicating that the Pt is present in its metallic state Pt(0). The binding energy values for the metallic Pt are in agreement with the literature data [20]. In order to identify the higher oxidation states of Pt, the spectrum has been curve fitted and the smaller doublets are detected at higher binding energy positions, i.e., at 72.0 and 75.2 eV, respectively, and reveal the existence of Pt(II) state (PtO species) in the catalyst. The percentage of these two species (Pt(0) and Pt(II)) are calculated from the relative intensities of these peaks and is shown in Table 2. The percentage of Pt(0) and Pt(II) species present in the

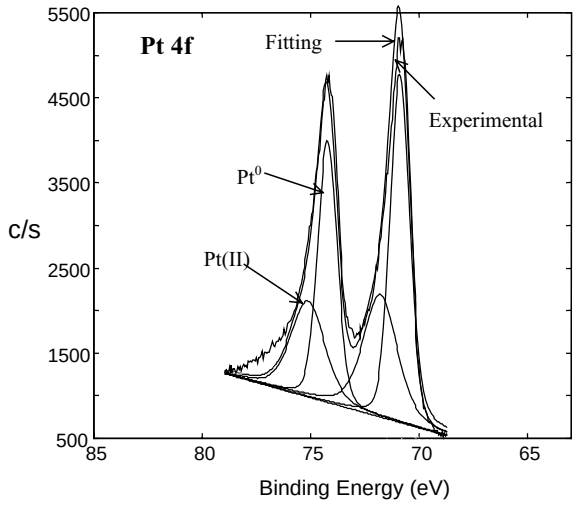

Fig. 3. XPS of Pt(4f) of the Pt/C-I nanocatalyst.

E-TEK catalyst is also compared in the Table 2. The relatively lower amount of Pt(0) species present in the Pt/C-I catalyst can be explained based on the fact that some of the fine bare Pt particles can always undergo easier oxidation, during the preparative process [21,22]. In addition, the surface Pt atomic compositions of these catalysts (Pt/C-I and E-TEK) are also compared in the Table 2. The slightly lower amount of Pt composition on the surface of the Pt/C-I catalyst than the nominal composition (20 wt.% of Pt) might be due to the relatively larger size and some degree of aggregation of the Pt particles as evident from the TEM picture (see Fig. 1a). However, it is difficult to make a detailed comparison of atomic composition of the Pt particles by using the XPS because this technique could analyze just only the top surface (5–10 nm in depth) of the sample. From the above results, it is realized that further investigations are needed to obtain higher amount of Pt in its metallic state and to enrich the surface atomic composition of Pt in the catalyst that must be essentially materialized without using any stabilizing agents.

3.3. Electrochemical characterization

Fig. 4 shows the first and second cycles of the CV recorded for the Pt/C-I catalyst in 0.1 M $HClO_4$ solution at a scan rate of 50 $mV\ s^{-1}$. In the first cycle, as soon as the forward scanning is started from −0.2 V, a higher hydrogen adsorption rate is noted. The hydrogen adsorption rate is more pronounced on the Pt nanoparticles; possibly because of the presence of highly reactive Pt(1 1 1) facets, which is evident from the observation of broad hydrogen adsorption–desorption features in the stabilized CV (see Fig. 5). Similarly, a higher hydrogen adsorption rate for an unsupported Pt nanocatalyst was observed, during the first cycle of CV in 6 M KOH solution in our previous work [23]. In the subsequent cycles, this higher hydrogen adsorption rate is drastically reduced because of the coverage of

Table 2
Surface Pt composition and different Pt species that are observed from the XPS for the Pt/C-I and 20 wt.% Pt/C E-TEK catalysts

Catalysts	Pt(0) species (%)	Pt(II) species (%)	Surface Pt composition (%)	Nominal Pt composition (%)
Pt/C-I	60.30	39.70	16	20
E-TEK	73.54	26.46	26	20

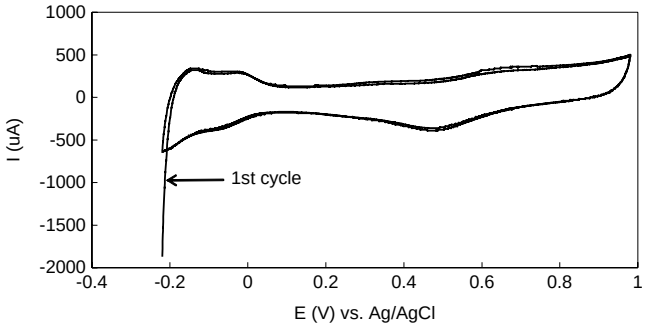

Fig. 4. First and second CV cycles for the Pt/C-I in 0.1 M $HClO_4$ at a scan rate of 50 mV s^{-1}.

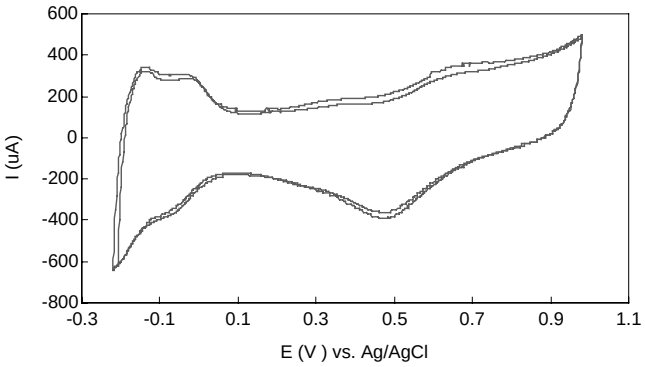

Fig. 5. Stabilized CV cycles for the Pt/C-I in 0.1 M $HClO_4$ at a scan rate of 50 mV s^{-1}.

hydrogen on the Pt particles, during the backward sweep of the first cycle.

The stabilized CV (11 and 20th cycles) curves for the Pt/C-I catalyst in 0.1 M $HClO_4$ is shown in Fig. 5. It is evident from the voltammograms that after the 10th cycle, the CV features are identical and the well defined hydrogen adsorption–desorption peaks are observed in the potential region −0.22 to 0.04 V, demonstrating a higher EAS area of the catalyst. In Table 3, the EAS area of the Pt/C-I catalyst is compared with that of the E-TEK catalysts, which has been measured in 0.5 M H_2SO_4, in our recent work [8]. We believe it is reasonable to make a comparison the EAS area of the Pt/C-I catalyst with our recent work because the loading level of Pt of the two catalysts viz., Pt/C-I and E-TEK on the GC electrode has been maintained constant, i.e., 48 μg cm^{-2}, and it is known that the influence of anions of the electrolyte in the low potential hydrogen adsorption–desorption region is always negligible.

Table 3
EAS area and I_{max} for the oxidation of 1 M CH_3OH for the Pt/C-I and 20 wt.% Pt/C E-TEK catalysts

Catalysts	Pt loading (μg cm^{-2})	EAS area (cm^2)	I_{max} of oxidation of 1 M CH_3OH (mA)
Pt/C-I	48	2.50	1.5
E-TEK[a]	48	2.87	0.9

[a] Taken from [8].

The values of the EAS area are obtained by measuring the charge from the hydrogen desorption peaks after subtracting the charge from the double-layer region and with the assumption that the smooth Pt electrode gives the hydrogen adsorption charge of 210 μC cm^{-2}. The EAS area of the Pt/C-I catalyst, which is determined by the magnitude of the hydrogen adsorption–desorption peaks, in turn, depends mainly on the size of the Pt particles and the presence of different crystallites of Pt, i.e., Pt(1 1 1), Pt(1 1 0) and Pt(1 0 0) facets [24,25]. Since the hydrogen adsorption–desorption peaks appear to be broad and featureless, it is presumed that the Pt(1 1 1) is the predominant facet in the Pt/C-I nanocatalyst [26]. Though the surface area of the Pt/C-I catalyst is less than the E-TEK, it is interesting to note that the EAS area of the Pt/C-I catalyst is almost similar to that of the E-TEK catalyst (see Tables 1 and 3). In order to understand this phenomenon, a more precise assignment of correlation of crystal plane orientation with the size of the particles has to be made.

In the stabilized CV curves, during the forward scanning, a pre-oxidation peak is observed at the potential region of ca. 0.3–0.35 V, which might be due to the formation of hydrous oxide as per the equation [23,27]:

$$Pt + xH_2O \leftrightarrow [Pt(OH)_x]^{2-} + xH^+ + ye \quad (2)$$

Burke et al. [27] suggested that these hydrous oxide species occur in the lower potential region (ca. at 0.4–0.5 V versus RHE in aqueous electrolytes) on highly active Pt adatoms (possess low coordination numbers with adjacent atoms) sites, which are usually formed on pre-cycling the electrode surface, during the anodic sweep. Here, it is reasonable to assume the possibility of formation of the hydrous oxide species in this lower potential region on the nanosize Pt particles that possess highly reactive low coordination number single crystals. The above discussion on the formation of hydrous oxide species assumed significance because of its involvement in the mediation of methanol oxidation reaction, which will be discussed in the following section.

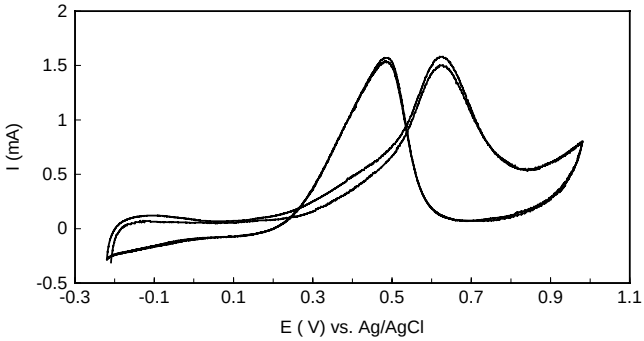

Fig. 6. CV for the Pt/C-I in 0.1 M $HClO_4$ + 1 M CH_3OH at a scan rate of 50 mV s^{-1}.

3.4. Electro-oxidation of methanol

Fig. 6 shows the CV recorded for the Pt/C–I catalyst in 0.1 M $HClO_4$ that contains 1 M CH_3OH (stabilized 5, 6th cycles). The onset of methanol oxidation takes place at potential ca. 0.3 V, and this onset potential for the methanol oxidation reaction coincides with the potential region for the formation of $[Pt(OH)_x]^{2-}$ species. Hence, it is obvious that these hydrous oxide species are involved in the mediation of methanol oxidation reaction. Frelink et al. [28] reported the formation active oxide species at lower potential region on the small sized Pt particles and suggested that these oxides favored the methanol oxidation reaction. The methanol oxidation current of the Pt/C-I is compared with the E-TEK catalyst (data taken from our recent work [8]) and is given in the Table 3. The methanol oxidation current of the Pt/C-I is found to be slightly higher than that of the E-TEK catalyst. This can be attributed to the reasons; (i) the FARM does not introduce any types of impurities to the catalytic sites during the preparative process. A similar view has also been stated by Valbuena et al. [14] in their preparation of the Pt-Ru/C nanocatalyst by using the FARM in an aqueous phase, and (ii) size of the Pt particles (3–4 nm) of the Pt/C-I nanocatalyst might be an optimum size for the enhanced methanol oxidation reaction. However, in order to have a deep understanding of the influence of these two factors, further investigations are required.

4. Conclusions

The 20 wt.% Pt/C nanocatalyst (Pt/C-I) has been synthesized by the simple FARM in THF solvent. The morphological results indicate that well-dispersed Pt nanoparticles with the diameter of 3–4 nm are obtained on the Vulcan XC-72 carbon support. It is inferred from the two different preparative approaches that the formation and dispersion of the Pt nanoparticles are favored by the THF solvent and high surface area of the Vulcan XC-72 carbon support. The surface characterization of the Pt/C-I catalyst reveals that 60.3% of Pt is present in its metallic form. Though the surface area of the Pt/C-I is lower than that of the 20 wt.% Pt/C E-TEK catalyst, the EAS area and methanol oxidation current of the Pt/C-I is almost similar and slightly higher than that of the E-TEK catalyst, respectively.

Acknowledgements

The work described in this paper was supported by a grant from the Research Grants Council (Project No. HKUST6193/01E) and a grant from the Innovation and Technology Commission (Project No. ITS/069/02) of Hong Kong SAR Government, China.

References

[1] S. Wasmus, A. Kuver, J. Electroanal. Chem. 461 (1–2) (1999) 14.
[2] X. Ren, P. Zelenay, S. Thomas, J. Davey, S. Gootesfeld, J. Power Sources 86 (1–2) (2000) 111.
[3] K.J. Klabunde (Ed.), Nanoscale Materials in Chemistry, Wiley, 2001, p. 1.
[4] T.J. Schmidt, M. Noeske, A.H. Gasteiger, R.J. Behm, P. Britz, W. Brijoux, H. Bonnemann, J. Electrochem. Soc. 145 (3) (1998) 1998.
[5] U.A. Paulus, U. Endruschat, G.J. Feldmeyer, T.J. Schmidt, H. Bonnemann, R.J. Behm, J. Catal. 195 (2000) 383.
[6] X. Wang, I.-M. Hsing, Electrochim. Acta 47 (2002) 2981.
[7] X. Zhang, Y.-K. Chan, Chem. Mater. 15 (2003) 451.
[8] J. Prabhuram, X. Wang, C.L. Hui, I.-M. Hsing, J. Phys. Chem. B 107 (2003) 11057.
[9] Z. Zhou, S. Wang, W. Zhou, G. Wang, L. Jiang, W. Li, S. Song, J. Liu, G. Sun, Q. Xin, Chem. Commun. (2003) 394.
[10] W.X. Chen, J.Y. Lee, Z. Liu, Chem. Commun. (2002) 2588.
[11] Z. Liu, X.Y. Ling, J.Y. Lee, X. Su, L.M. Gan, J. Mater. Chem. 13 (2003) 3049.
[12] T.C. Deivaraj, W. Chen, J.Y. Lee, J. Mater. Chem. 13 (2003) 2555.
[13] B. Yang, Q. Lu, Y. Wang, L. Zhuang, J. Lu, P. Liu, Chem. Mater. 15 (2003) 3552.
[14] W.H.L. Valbuena, D.C.D. Azevedo, E.R. Gonzalez, Electrochim. Acta, in press.
[15] H. Bonnemann, W. Brijoux, R. Brinkmann, R. Fretzen, T. Joussen, R. Koppler, B. Korall, P. Neiteler, J. Richter, J. Mol. Catal. 86 (1994) 129.
[16] H. Bonnemann, W. Brijoux, R. Brinkmann, E. Dinjus, T. Jouben, B. Korall, Angew. Chem. Int. Ed. Engl. 30 (1991) 1312.
[17] E. Antolini, J. Mater. Sci. 38 (2003) 2995.
[18] M. Uchida, Y. Aoyama, M. Tanabe, N. Yanagihara, N. Eda, A. Ohta, J. Electrochem. Soc. 142 (1995) 2572.
[19] J. McBreen, H. Olender, S. Srinivasan, K. Kordesch, J. Appl. Electrochem. 11 (1981) 787.
[20] S. Hufner, G.K. Wertheim, Phys. Rev. B 11 (1975) 678.
[21] A.K. Shukla, M. Neergat, P. Bera, V. Jayaraman, S.M. Hegde, J. Electroanal. Chem. 504 (2001) 111.
[22] A.S. Arico, P. Creti, E. Modica, G. Monforte, V. Baglio, V. Antonucci, Electrochim. Acta 45 (2000) 4319.
[23] J. Prabhuram, R. Manoharan, J. Power Sources 74 (1998) 54.
[24] K. Kinoshita, D.R. Ferrier, P. Stonehart, Electrochim. Acta 23 (1978) 45.
[25] P.N. Ross, Electrochim. Acta 36 (1991) 2053.
[26] J.M. Feliu, J.M. Orts, A. Fernandez-Vega, A. Aldez, J. Electroanal. Chem. 296 (1990) 191.
[27] L.D. Burke, M.B.C. Roche, W.A. O'Leary, J. Appl. Electrochem. 18 (1988) 781.
[28] T. Frelink, W. Visscher, J.A.R. Van Veen, J. Electroanal. Chem. 382 (1995) 65.